Journal of Integrative Neuroscience

J. Integr. Neurosci. **2026**; 25(4): 47565
https://doi.org/10.31083/JIN47565

Original Research

Atractylodin Suppresses Fibrotic Scar Formation and Enhances Functional Recovery Following Spinal Cord Injury

Zhenwei Li[1,2,†], Chao Fang[1,2,†], Chengcheng Feng[1], Zuomeng Wu[1,2], Chenhao Zhao[1,2], Cailiang Shen[1,2,3,*]

[1]Department of Orthopedics, The First Affiliated Hospital of Anhui Medical University, 230032 Hefei, Anhui, China
[2]Laboratory of Spinal and Spinal Cord Injury Regeneration and Repair, The First Affiliated Hospital of Anhui Medical University, 230032 Hefei, Anhui, China
[3]Anhui Province Research Center for the Clinical Application of Digital Medical Technology, The First Affiliated Hospital of Anhui Medical University, 230022 Hefei, Anhui, China
*Correspondence: shencailiang@ahmu.edu.cn (Cailiang Shen)
[†]These authors contributed equally.
Academic Editor: Nuno A. Silva
Submitted: 21 October 2025 Revised: 7 December 2025 Accepted: 23 December 2025 Published: 22 April 2026

Abstract

Background: Fibrous scar formation significantly inhibits axonal regeneration and functional recovery following spinal cord injury (SCI). Atractylodin (ATD), an active constituent of traditional Chinese medicine, exhibits broad pharmacological properties, including anti-inflammatory and anti-fibrotic effects. Nevertheless, the potential therapeutic role of ATD in SCI and its underlying molecular mechanisms remain to be fully elucidated. **Methods**: An SCI model was established in C57 mice. Motor function was assessed using the Basso Mouse Scale scoring system, inclined plane test, swimming test, and footprint analysis. Immunohistochemical staining was performed to evaluate fibrotic scar formation and neuronal survival. Western blotting and quantitative real-time PCR (qPCR) were also employed to investigate the molecular mechanisms underlying ATD-mediated regulation of fibroblasts following SCI. **Results**: ATD administration significantly enhanced motor function in SCI mice, reduced the area of fibrotic scars, and suppressed the expression of fibrotic markers. Mechanistically, ATD inhibited Mothers Against Decapentaplegic Homolog 2/3 (SMAD2/3) phosphorylation and nuclear translocation, thereby suppressing fibroblast activation and extracellular matrix deposition, while promoting neuronal survival and axonal regeneration. **Conclusions**: ATD mitigates fibrotic scar formation by targeting the Transforming Growth Factor Beta (TGF-β)/SMAD pathway, thereby facilitating axonal regeneration and functional recovery. This offers a promising therapeutic strategy for SCI.

Keywords: spinal cord injuries; atractylodin; fibrosis; transforming growth factor beta; smad proteins

1. Introduction

Spinal cord injury (SCI) is a profoundly disabling condition characterized by acute onset and catastrophic outcomes. Its clinical refractoriness creates a significant burden for patients, their families, and society at large [1]. Currently, no efficacious treatment is available for SCI [2]. In the acute stage, extensive neuronal death at the lesion epicenter triggers microglial/macrophage recruitment [3,4]. These cells engulf cellular debris, secrete numerous cytokines and inflammatory mediators, and recruit astrocytes and fibroblasts to participate in the subsequent repair process [5–7]. This cascade establishes an inflammatory microenvironment at the injury site. As astrocytes and fibroblasts undergo reactive activation, they secrete substantial amounts of chondroitin sulfate proteoglycans (CSPGs) and extracellular matrix (ECM) proteins, resulting in the formation of dense fibrous and glial scars at the periphery of the lesion [8–10]. These scars significantly impede axonal regeneration and functional recovery. While fibrotic scar formation may have a protective role, it is increasingly recognized that excessive deposition after SCI is ultimately detrimental. Therefore, its moderate inhibition is considered a promising strategy to support neural repair and functional restoration [11,12]. Therefore, targeting fibrotic scar formation after SCI may represent an effective strategy to reduce neuron death and promote axon regeneration and functional recovery.

The Transforming Growth Factor Beta/Mothers Against Decapentaplegic Homolog (TGF-β/SMADs) signaling pathway serves as a central regulator in the development of tissue fibrosis and is extensively implicated in key pathological processes, including ECM remodeling, fibroblast activation, and fibrotic scar formation [13–15]. Upon binding to its receptor, TGF-β activates transmembrane serine/threonine kinase receptors, leading to the phosphorylation of SMAD2/3. It interacts with SMAD4 to assemble a transcriptional regulator complex. This complex then enters the nucleus, where it directly modulates the expression of key fibrosis-related genes, including those encoding collagen, fibronectin, and α-

smooth muscle actin (α-SMA) [16,17]. Dysregulation of this pathway is a key driver of progressive tissue sclerosis in diverse fibrotic diseases, including those affecting the liver, lungs, and kidneys [18–20]. Following SCI, significantly upregulated expression of TGF-β1 occurs in the local microenvironment, which promotes the phenotypic transition of spinal cord fibroblasts toward a pro-fibrotic state through activation of the SMADs signaling cascade. Concurrently, TGF-β1 suppresses the activity of matrix metalloproteinase (MMP) and upregulates the expression of tissue inhibitors of metalloproteinases (TIMPs), resulting in excessive ECM accumulation and the formation of a dense, fibrotic scar barrier [21,22]. This pathological structure impedes axonal regeneration and actively suppresses neural repair through both physical and chemical barrier mechanisms. Therefore, targeted modulation of the TGF-β/SMADs signaling pathway represents a promising therapeutic strategy to attenuate fibrotic scar formation following SCI and facilitate nerve regeneration.

Atractylodin (ATD) is a polyacetylene compound extracted from the dried rhizome of Atractylodes lancea or Atractylodes chinensis, which are members of the Asteraceae family in traditional Chinese medicine [23]. ATD has important and extensive pharmacological effects. It has been found to play an anti-inflammatory role by inhibiting pro-inflammatory factors and the NF-κB pathway, thereby improving intestinal inflammation [24,25]. In addition, ATD can activate the AMPK/SIRT1 signaling pathway, enhance autophagy and inhibit IL-1β-induced apoptosis of chondrocytes, thus delaying the progression of osteoarthritis [26]. In the field of metabolic diseases, ATD can significantly reduce lipid deposition by promoting the browning of white adipocytes and up-regulating the expression of uncoupling protein 1 (UCP1). ATD offers therapeutic potential for obesity, type 2 diabetes and non-alcoholic fatty liver disease [27–29]. Recent studies have also demonstrated the value of ATD in the prevention of pulmonary fibrosis by stabilizing vimentin and inhibiting the recycling of TGF-β1 [30]. Although ATD has a variety of biological activities, its therapeutic effect on SCI has not been studied, and the specific mechanism is unclear.

Therefore, we sought to determine if ATD-mediated inhibition of fibrous scar formation enhances neurological recovery in a mouse model of SCI and, further, to uncover the mechanistic basis of this effect through *in vitro* experiments. We hypothesized that ATD reduces the formation of fibrous scar tissue after SCI by inhibiting TGF-β/SMADs signaling. This study provides evidence that ATD is a safe and promising therapeutic agent for the clinical treatment of SCI.

2. Methods and Materials

2.1 Animals

Female C57BL/6 mice (8–10 weeks old, 20–22 g weight) were supplied by the Animal Center of Anhui Medical University, China. The animals were acclimatized and housed under standard specific pathogen-free conditions (22 °C, 30–50% humidity, 12-h light/dark cycle; 4 mice/cage) with free access to food and water. After final assessments, all mice were humanely euthanized with carbon dioxide. Animal surgeries were performed under the same approved protocol as a prior study investigating a different therapeutic compound and mechanism.

2.2 Establishment of the SCI Model and ATD Treatment

Mice were randomly assigned to the sham operation group, vehicle group, or ATD treatment group. SCI was induced using a severe compression model. Briefly, after anesthesia induction with intraperitoneal 1% pentobarbital sodium (MERCK, Rahway, NJ, USA, CAS:57-33-0), mice underwent a T9–T10 laminectomy to expose the spinal cord. The exposed cord was then subjected to a 5-second compression using a calibrated Dumont #5 forceps (Fine Science Tools, Heidelberg, Germany, Cat1125220). The muscle and skin layers were then sutured sequentially. Postoperatively, all mice received antibiotic treatment to prevent infection and manual bladder expression twice daily until spontaneous urination was restored. Mice in the sham group underwent a laminectomy without spinal cord compression. The ATD treatment group received daily intraperitoneal injections of 20 or 40 mg/kg ATD (MCE, New Jersey, USA, HY-N0238) starting immediately after injury and continuing until day 7 post-injury. The vehicle group received an equivalent volume of the solvent to control for potential solvent-related effects. All surgical procedures were performed by a single, experienced, and independent surgeon to ensure consistency and minimize procedural variability.

2.3 Motor Function Score

Hindlimb motor function was assessed using the Basso Mouse Scale (BMS) score, the slant board test and footmark analysis test, as described previously. Mice were placed in an open field, and their hind limb movement was observed before operation and at 1, 3, 7, 14, 21, and 28 days post-injury (dpi). The footprint analysis test was conducted at 28 dpi to further evaluate the recovery of motor function. The front and back paws were soaked in green and red dyes, respectively, and the animals were placed on white paper to walk. All assessments were conducted in a blinded fashion by two independent, experienced investigators to ensure objectivity.

2.4 H&E and Nissl Staining

After the accomplishment of the necessary assessments, all mice were euthanized using carbon dioxide. The flow rate of CO_2 should be controlled at 50% of the volume of the euthanasia chamber per minute. The animals should be exposed to CO_2 for at least 5 minutes. Mice were transcardially perfused with 0.9% saline and then

4% paraformaldehyde (PFA) (Servicebio, Wuhan, Hubei, China, G1101). The spinal cord segment encompassing the injury epicenter was dissected and post-fixed overnight in 4% PFA at 4 °C. After sucrose gradient cryoprotection, the specimens were embedded in paraffin wax. Subsequently, longitudinal sections were cut at 5 µm for the following histological analyses. For hematoxylin and eosin (H&E) staining, sections first underwent hematoxylin staining for 5 minutes, were sequentially rinsed with double-distilled water, and were then subjected to eosin counterstaining for 1 minute. Digital images were acquired under a light microscope. Sections designated for Nissl staining were stained using a Nissl stain solution (Beyotime, Shanghai, China, C0117) at 37 °C for a duration of 10 minutes, briefly washed with double-distilled water, differentiated with 95% ethanol for 5 seconds, and then dehydrated and cleared as appropriate. Representative images were captured using a light microscope VS200 Panoramic Tissue Quantitative Analysis System (OLYMPUS, Tokyo, Japan, VS200). Positive Nissl staining was identified by the presence of distinct, dark purple granules (Nissl bodies) within the neuronal cytoplasm. Viable motor neurons with large, clear nuclei and rich Nissl substance were counted.

2.5 Immunofluorescence Staining

For immunofluorescence, mice were transcardially perfused with 4% paraformaldehyde, and the spinal cord tissues were harvested and processed for paraffin embedding. Prior to staining, the sections underwent deparaffinization in xylene and sequential rehydration through a graded alcohol series to aqueous conditions. Antigen retrieval was performed using citrate buffer (pH 6.0), followed by blocking with 5% bovine serum albumin (BSA) (Servicebio,Wuhan, Hubei, China, GC305010) in phosphate-buffered saline (PBS) for 1 h at room temperature to reduce nonspecific binding. To label astrocytes and neurons, sections were incubated overnight at 4 °C with rabbit anti-Glial Fibrillary Acidic Protein (GFAP) antibody (1:1000; Abcam, Cambridge Biomedical Campus, Cambridge, UK, ab68428) and rabbit anti-TUJ1 antibody (1:1000; Abcam, ab18207), respectively. Sections then received fluorescent secondary antibodies for detection: green-fluorescent Alexa Fluor 488 goat anti-rabbit Ig (Gat 1:50 from Elabscience, Wuhan, Hubei, China, E-AB-1055) and red-fluorescent Cy3 goat anti-mouse IgG (Gat 1:50 from Elabscience, E-AB-1011). Nuclei were counterstained with 4′,6-diamidino-2-phenylindole (DAPI) (Beyotime, Shanghai, China, P0131) Fluorescent signals were visualized and images captured using a Leica DM-6B fluorescence microscope (Leica, Wetzlar, Hesse, Germany, DM-6B). For quantification of positive cells or stained areas, digital images were analyzed using ImageJ software (1.54r, NIH, Bethesda, MD, USA). Quantification data are presented as mean ± Standard Deviation (SD) (n = 6 mice per group). For each animal, three non-adjacent sections were analyzed, and from each section, three random fields within the lesion border zone were quantified and averaged.

2.6 TUNEL Staining

Mice were transcardially perfused for tissue fixation, and paraffin-embedded tissue sections were subsequently prepared. Tissue sections were deparaffinized and rehydrated through a xylene-alcohol series, followed by antigen retrieval in citrate buffer. Subsequently, nonspecific binding was blocked by incubation with 5% BSA for 1 hour at room temperature. Apoptosis was then assessed by terminal deoxynucleotidyl transferase-mediated 2′-Deoxyuridine-5′-Triphosphate (dUTP) nick-end labeling (TUNEL) staining, which was carried out accordingly to the manufacturer's instructions (Beyotime, C1089).

2.7 Cell Culture and Processing

Primary fibroblasts derived from mouse spinal cord were acquired from Procell. Cells were expanded in the provided complete growth medium (Procell, Wuhan, Hubei, China, CM-M162) according to the supplier's instructions. All cultures were kept in a humidified incubator at 37 °C with 5% CO_2. Primary fibroblasts were characterized by vimentin immunofluorescence staining, confirming a purity of >90%. The cells were confirmed to be free of contamination from human immunodeficiency virus type 1 (HIV-1), hepatitis B virus (HBV), hepatitis C virus (HCV), mycoplasma, as well as bacterial, fungal, and yeast pathogens. Cells were pretreated with ATD at a concentration of 100 µM for 24 h, with the compound dissolved in 0.1% Dimethyl Sulfoxide (DMSO) as vehicle control. Subsequently, fibroblasts were stimulated with TGF-β (100 ng/mL, MedChemExpress, Monmouth Junction, NJ, USA, HY-P70648) for an additional 24 h to induce activation.

2.8 CCK-8 Analysis

We seeded the fibroblasts into 96-well plates (5×10^3 cells in 100 µL per well) and cultured them for 24 h at 37 °C in a humidified 5% CO_2 atmosphere. Following drug treatment, 10 µL of CCK-8 solution (Beyotime, Shanghai, China, C0037) was added to each well, and the cells were further incubated for 2 h. Following incubation, the optical density at 450 nm was recorded using a LUX multimodal microplate reader (Thermo Fisher Scientific, Waltham, MA, USA, VLBL00GD2). Cell viability was then expressed as a percentage relative to the control groups.

2.9 Western Blot

For Western blot analysis, proteins were extracted from cells or tissue samples using RIPA lysis buffer (Beyotime, P0013B). Following lysis, the protein concentration was quantified with a BCA assay kit (Beyotime, P0010) prior to further processing. After separation by

SDS-PAGE (20 µg protein per lane) and transfer to PVDF membranes, the membranes were incubated in a blocking buffer (5% non-fat milk in Tris-Buffered Saline with Tween® 20 (TBST) (Servicebio, Wuhan, Hubei, China, G0001)) for 2 h at room temperature. This was followed by an overnight incubation at 4 °C with the respective primary antibodies. Membranes then received incubation with the appropriate HRP-conjugated secondary antibodies for 2 hours at room temperature. Detailed information for all antibodies involved in WB: FN (1:1000, Immunoway, SuZhou, JiangSu, China, YM8309), Collagen (1:1000, Immunoway, YT6135), α-SMA (1:1000, Immunoway, YM8040), GAPDH (1:1000, Immunoway, YM8016), TGF-β (1:1000, Immunoway, YM8257), P-SMAD2/3 (1:1000, Immunoway, YM8550), SMAD2/3 (1:1000, Immunoway, YT4332), SMAD4 (1:1000, Immunoway, YM8370), SMAD7 (1:1000, Immunoway, YN2330), Goat Anti Rabbit IgG(H+L) (HRP) (1:10,000, Immunoway, RS0002). Immunoreactive bands were detected using WesternBright ECL HRP substrate (Advansta, San Jose, CA, USA, K-12045-D20) at room temperature. To quantify protein expression, the optical density of each band was measured using ImageJ and normalized to its corresponding loading control.

2.10 Reverse Transcription Quantitative Polymerase Chain Reaction (RT-qPCR)

At 14 days post-injury, mice were perfused, and a 5-mm segment of spinal cord tissue centered precisely on the injury epicenter was dissected under a surgical microscope. This segment, encompassing the primary lesion and perilesion area, was immediately snap-frozen for subsequent total RNA extraction. RNA was extracted from tissues, cells, and exosomes with TRIzol reagent (Gibco, Grand Island, NY, USA, 15596026CN). For cDNA synthesis, the Superscript III RT Reaction Mix (Invitrogen, Carlsbad, CA, USA, 18080085) was used. Quantitative PCR was performed with SYBR Green PCR Master Mix on a 7900 Fast Real-Time PCR System (7900, Applied Biosystems, Foster City, CA, USA). Relative gene expression was determined by normalizing to GAPDH and applying the $2^{-\Delta\Delta CT}$ calculation. The primer sequences were listed below:

Fn: 5′–CCATTCCACCTTACAACAC–3′, 5′–CAAGCCAGACACAACAAT–3′;

Col1α1: 5′–GTGAGACAGGCGAACAAG–3′, 5′–CCAGGAGAACCAGGAGAA–3′;

GAPDH: 5′–*TGTCTCCTGCGACTTCAACA*–3′, 5′–GGTGGTCCAGGGTTTCTTACT–3′.

2.11 Statistical Analyses

All statistical analyses were performed with SPSS (version 16.0; IBM, Chicago, IL, USA) and GraphPad Prism (version 8.0, GraphPad Software, Boston, MA, USA). Quantitative data are expressed as means ± SD. Differences were considered statistically significant based on a two-tailed Student's *t*-test (for two-group comparisons) or one-way ANOVA with Tukey's post hoc test (for multi-group comparisons), as appropriate. For non-parametric data, the Mann–Whitney U test (two-group comparison) or Kruskal-Wallis test with Dunn's post hoc test (multiple comparisons) was used. A p-value < 0.05 was defined as the threshold for statistical significance.

3. Results

3.1 ATD Promotes the Recovery of Motor Function After SCI

To evaluate the therapeutic efficacy of ATD after SCI, mice underwent surgical induction of SCI followed by intraperitoneal administration of ATD post-operation (Fig. 1A). A series of behavioral assessments were subsequently performed to evaluate functional recovery, with the experimental timeline summarized in Fig. 1B. Recovery of motor function represents a critical endpoint for assessing therapeutic outcomes. Therefore, locomotor performance was systematically evaluated using the Basso Mouse Scale (BMS) at multiple time points post-injury. Mice in the ATD-treated groups exhibited significantly improved motor function starting on day 14 after SCI, with the most pronounced recovery observed in the high-dose group (Fig. 1C,D). Consistent with these findings, swimming test results demonstrated enhanced hindlimb motor coordination and propulsion in the ATD treatment groups compared to the vehicle group, particularly in the high-dose cohort (Fig. 1E,F). Footprint analysis confirmed that ATD treatment led to improved gait symmetry and stride patterns, indicating enhanced functional recovery of both hindlimbs (Fig. 1G–I). Collectively, these data demonstrate that ATD promotes robust recovery of motor function following SCI in mice.

3.2 ATD Inhibits Fibrous Scar Formation After SCI

Following SCI, astrocytes and fibroblasts collaborate to form a dense glial-fibrotic scar surrounding the lesion core, which acts as a major barrier to axonal regeneration. This study further investigated the impact of ATD on glial-fibrotic scar formation after SCI (Fig. 2A). Quantitative real-time PCR (qPCR) analysis revealed that ATD treatment significantly downregulated the mRNA expression levels of key fibrosis-related markers, *Fn* and *Col1α1*, with a clear dose-dependent effect (Fig. 2B,C). Immunofluorescence staining demonstrated that at 14 dpi, ATD administration markedly reduced the protein expression of fibrotic components including FN, Collagen, and α-smooth muscle actin (α-SMA), along with a significant decrease in the fibroblast-specific marker PDGFRβ (Fig. 2D–K). Furthermore, fluorescence-based analysis at 28 days post-treatment showed substantially lower fibronectin expression and a reduced area of fibrotic scarring in the ATD-treated groups (Fig. 2L,M). Compared to the vehicle control group, ATD treatment significantly diminished the GFAP-

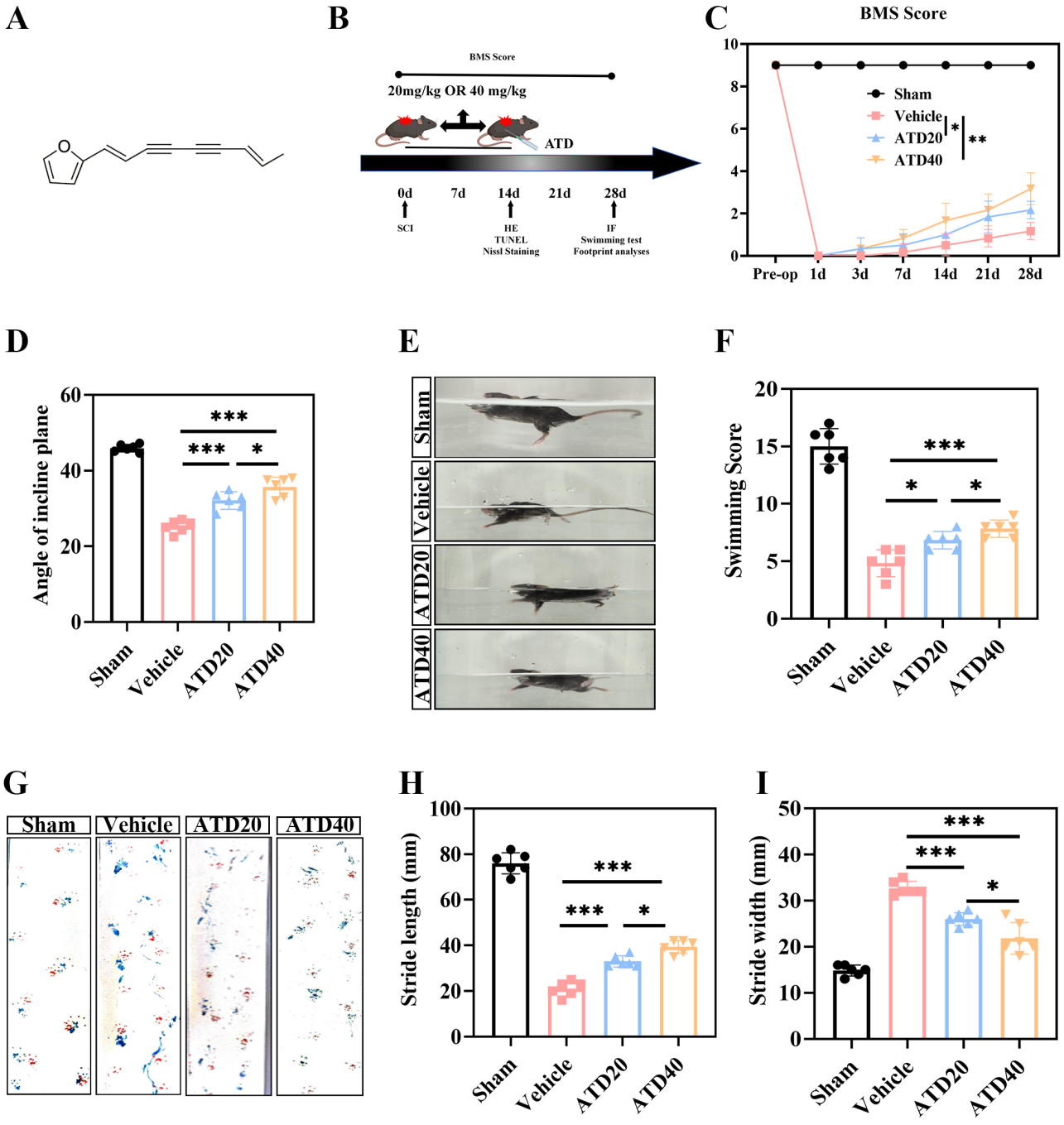

Fig. 1. Atractylodin significantly improve the motor function of mice after SCI. (A) Chemical structure of ATD. (B) Schematic representation of the timeline for behavioral experiments conducted at various time points following SCI. (C) Results from the BMS test showing the recovery of hindlimb motor function after SCI (n = 12 animals per group). (D) Results from the Santing board test showing recovery of hindlimb motor function after SCI (n = 6 in each group). (E,F) Results from the swimming test showing recovery of hindlimb motor function after SCI (n = 6 in each group). (G–I) Results from footprint analysis showing the recovery of hindlimb motor function after SCI (n = 6 in each group). Data shown are the mean ± SEM, *$p < 0.05$, **$p < 0.01$, ***$p < 0.001$. SCI, spinal cord injury; ATD, atractylodin; BMS, Basso Mouse Scale; SEM, Standard Error of the Mean.

positive glial scar region at 28 dpi. Notably, the structural integrity of the glial-fibrous scar interface was disrupted, with loss of tight apposition between glial and fibrotic compartments, indicating impaired scar continuity (Fig. 2L,N). Collectively, these findings demonstrate that ATD effectively narrows the spatial extent of the glial-fibrotic scar boundary and reduces the overall scar volume after SCI, thereby creating a more permissive microenvironment for axonal regrowth. Moreover, histopathological evaluation by H&E staining revealed no apparent abnormalities in vital

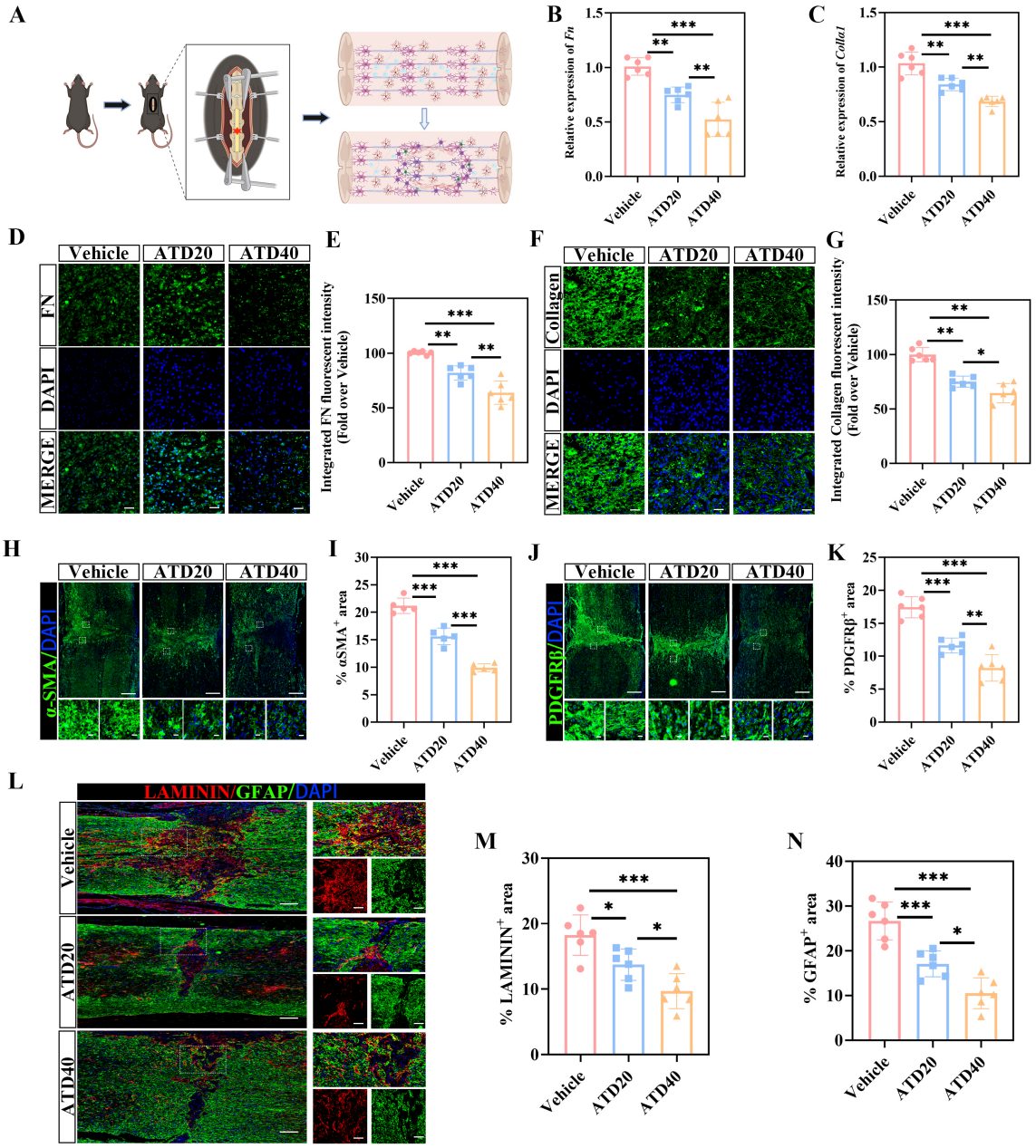

Fig. 2. Atractylodin inhibits fibrous scar formation following SCI. (A) Schematic illustration of fibrous glial scar formation in the injured spinal cord of mice following SCI modeling. (B) Quantitative gene expression analysis of *Fn* at the lesion center in the Vehicle, ATD20, and ATD40 groups at 14 dpi (n = 6 animals per group). (C) Quantitative gene expression analysis of *Col1α1* at the lesion center in the Vehicle, ATD20, and ATD40 groups 14 days after SCI (n = 6 animals per group). (D,E) Immunofluorescence staining and quantitative assessment of FN distribution around the injury site in the Vehicle, ATD20, and ATD40 groups at 14 dpi (n = 6 animals per group; scale bar = 100 μm). (F,G) Immunofluorescence staining and quantitative analysis of collagen deposition around the injury site in the three experimental groups at 14 dpi (G) (n = 6 animals per group; scale bar = 100 μm). (H,I) Immunofluorescence staining and quantification of α-SMA expression around the injury region in the Vehicle, ATD20, and ATD40 groups at 14 dpi (n = 6 animals per group; scale bar = 500 μm, enlarged view scale bar = 50 μm). (J,K) Immunofluorescence staining and quantitative evaluation of PDGFRβ in peri-lesion areas of all groups at 14 dpi (n = 6 animals per group; scale bar = 500 μm, enlarged view scale bar = 50 μm). (L–N) Immunofluorescence staining and quantitative analysis of LAMININ and GFAP-positive areas around the injury site in the Vehicle, ATD20, and ATD40 groups at 28 dpi (n = 6 animals per group; scale bar = 500 μm, enlarged view scale bar = 100 μm). Data shown are the mean ± SEM, *$p < 0.05$, **$p < 0.01$, ***$p < 0.001$.

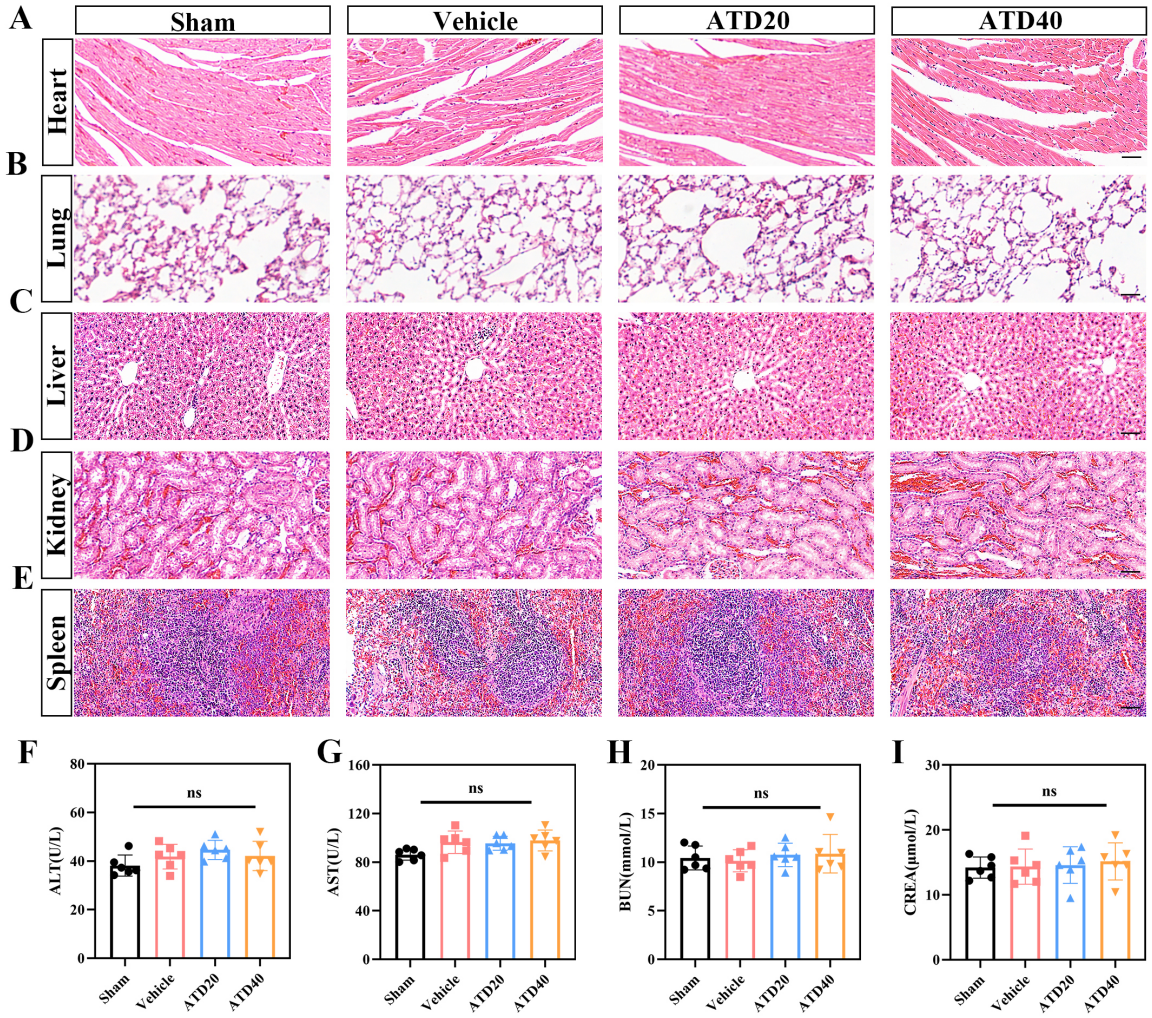

Fig. 3. Atractylodin exhibits favorable biocompatibility *in vivo*. (A–E) Histopathological analysis (H&E staining) of major organs was performed on day 28 after SCI. No significant pathological alterations were observed in the heart (A), lungs (B), liver (C), kidneys (D), or spleen (E) across the sham, Vehicle, ATD20, and ATD40 groups. All tissue sections displayed normal architecture and cellular morphology, with no signs of inflammation, necrosis, or tissue damage (n = 6 animals per group; scale bar = 100 μm). (F–I) Evaluation of systemic biosafety via serum biochemistry. At 7 days post-injury, key markers for hepatic and renal function were measured. Serum levels of (F) alanine aminotransferase (ALT), (G) aspartate aminotransferase (AST), (H) blood urea nitrogen (BUN), and (I) creatinine (CRE) showed no significant differences among the sham, Vehicle, ATD20, and ATD40 groups (n = 6 animals per group). ns $p > 0.05$.

organs, including the heart, liver, spleen, lung, and kidney, after 28 days of ATD treatment (Fig. 3A–E), suggesting a favorable safety profile under the experimental conditions used. To comprehensively evaluate the *in vivo* biosafety of ATD, we performed serum biochemical analysis on blood samples collected at 7 dpi. Key markers of hepatic and renal function—alanine aminotransferase (ALT), aspartate aminotransferase (AST), blood urea nitrogen (BUN), and creatinine (CRE)—were quantified across all experimental groups (Fig. 3F–I). Compared to the Sham group, the SCI+Vehicle group showed no significant increase in any of these markers, indicating that the injury itself did not induce overt hepatic or renal dysfunction at this time point. Crucially, mice treated with either dose of ATD (20 or 40 mg/kg) exhibited serum levels of ALT, AST, CRE, and BUN that were statistically indistinguishable from both the Sham and SCI+Vehicle controls (Fig. 3F–I). All measured values remained within established normal physiological ranges. These data demonstrate that ATD administration at the therapeutic doses used in this study did not elicit detectable hepatotoxicity or nephrotoxicity.

3.3 ATD Can Reduce Neuronal Apoptosis and Promote Axonal Repair After SCI

We investigated the effects of ATD on the dynamic regulation of neurons and axons following SCI. H&E staining and Nissl staining were performed on spinal cord tissue sections to assess structural integrity and neuronal morphological changes after injury. The results revealed exten-

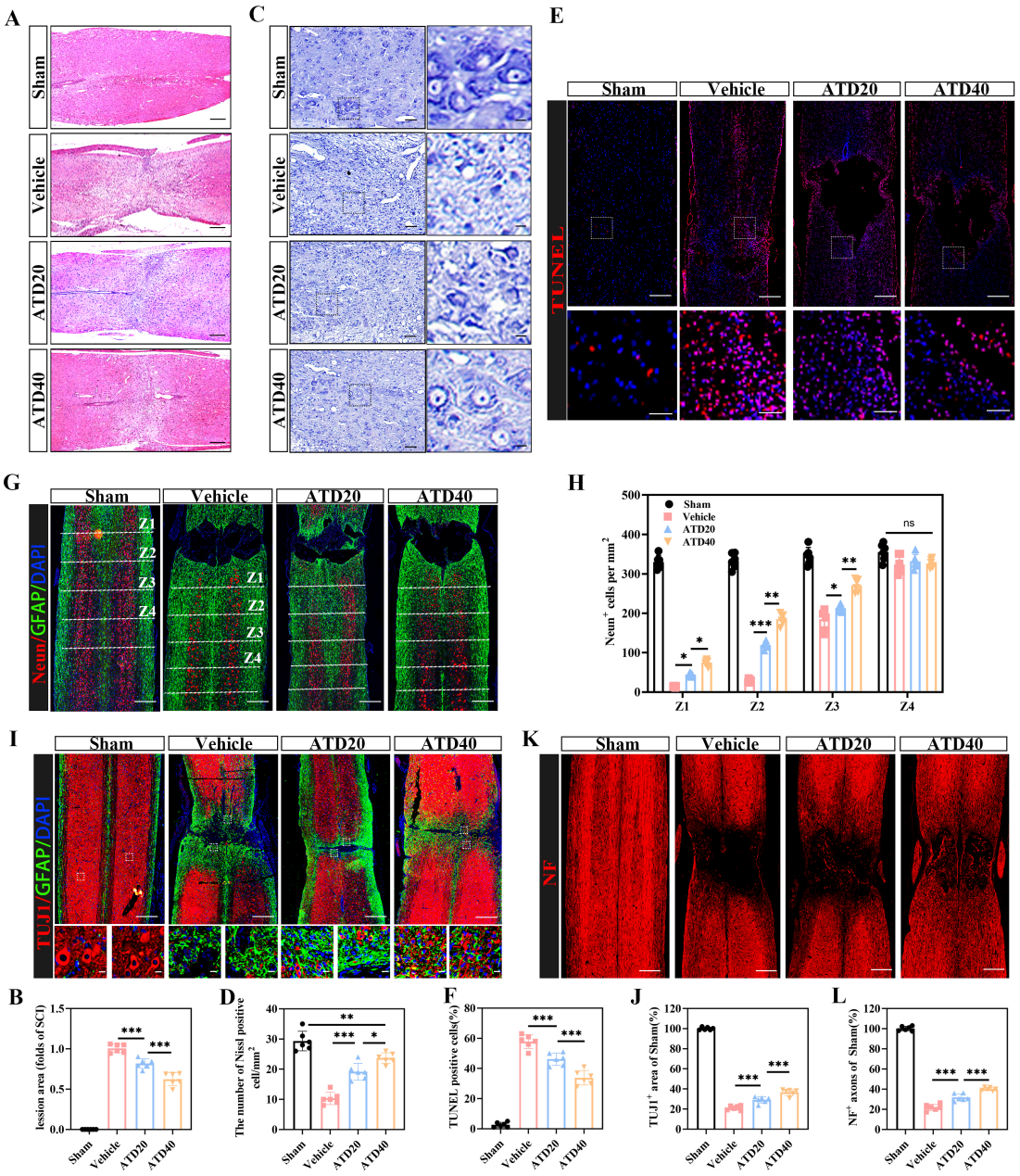

Fig. 4. Atractylodin inhibits neuronal apoptosis and promotes axonal regeneration following SCI. (A) Representative H&E-stained images of the lesion area at 28 days post-SCI in Sham, Vehicle, ATD20, and ATD40 groups (scale bar = 500 μm). (B) Corresponding quantitative analysis of lesion size from panel (A). (n = 6 animals per group). (C) Nissl staining was used to evaluate the morphological integrity and distribution of Nissl-positive neurons in the injured spinal cord tissues across all experimental groups at 28 dpi (scale bar = 100 μm, enlarged view scale bar = 20 μm). (D) Quantitative analysis of the number of Nissl-positive neurons from panel (C) (n = 6 animals per group). (E) Representative images of TUNEL assay detecting apoptotic cells in the lesion area (scale bar = 500 μm, enlarged view scale bar = 100 μm). (F) Quantification of TUNEL-positive cells from panel (E) (n = 6 animals per group). (G) Immunofluorescence labeling of $NeuN^+$ neurons was performed to assess neuronal survival (scale bar = 500 μm). (H) Quantification of $NeuN^+$ neuron counts from panel (G) (n = 6 animals per group). (I) Representative double immunofluorescence images of TUJ1+ axons (green) and GFAP+ astrocytes (red) (scale bar = 500 μm, enlarged view scale bar = 20 μm). (J) Quantification of the relative positive areas of TUJ1 and GFAP from panel (I). (K) Immunofluorescence images showing NF+ neurofilaments (regenerating axons) in the injured spinal cord (scale bar = 500 μm). (L) Quantified fluorescence intensity of NF+ signals from panel (K). (n = 6 animals per group). Data shown are the mean ± SEM, *$p < 0.05$, **$p < 0.01$, ***$p < 0.001$, ns $p > 0.05$.

sive neuron loss and cavity formation at the lesion epicenter in SCI mice. The Vehicle group displayed characteristic features of severe neurodegeneration, such as neuronal pyknosis, Nissl body disintegration, and nuclear dissolution. These pathological features were substantially alleviated by ATD treatment (Fig. 4A–D). Next, TUNEL staining combined with NeuN immunofluorescence was conducted to evaluate neuronal apoptosis and survival. In the sham group, neurons were regularly aligned and showed minimal apoptotic activity. In stark contrast, the SCI group suffered substantial neuronal loss, disorganized cytoarchitecture, and extensive apoptosis. However, ATD treatment markedly increased the number of surviving NeuN-positive neurons in the peri-lesion areas (Z1–Z3) compared to the Vehicle group (Fig. 4E–H). Collectively, these results indicate that ATD potently inhibits neuronal apoptosis and promotes neuronal survival following SCI. To investigate whether ATD further contributes to axonal regeneration by attenuating fibrotic scarring, we performed immunofluorescence staining for TUJ1 and NF at 28 dpi. Quantitative analysis revealed that four weeks of ATD treatment significantly expanded the area of TUJ1-positive labeling relative to the Vehicle group (Fig. 4I,J), implying the promotion of axonal sprouting. Furthermore, the ATD group exhibited a marked increase in the number of NF-positive axons penetrating the lesion core (Fig. 4K,L), indicating successful axonal regeneration across the scar boundary.

3.4 ATD Inhibited TGF-β-Induced Fibrogenesis in Fibroblasts

To investigate the anti-fibrotic effects of ATD on spinal cord fibroblasts, we first confirmed its biocompatibility. The CCK-8 assay revealed no significant cytotoxicity at a concentration of 100 μM (Fig. 5A). We then modeled fibrotic activation using TGF-β stimulation. While TGF-β significantly upregulated the mRNA expression of the key fibrosis-related genes *Fn* and *Col1α1*, ATD treatment effectively suppressed this induction (Fig. 5B,C). At the protein level, Western blot analysis confirmed that TGF-β markedly increased the expression of FN, Col1α1, and α-SMA, all of which were suppressed by ATD in a concentration-dependent manner (Fig. 5D–G). For all original Western blot figures of Fig. 5D, see **Supplementary Material**. Consistent with these findings, immunofluorescence staining demonstrated that TGF-β induced robust fibroblast activation, characterized by increased α-SMA expression and cytoskeletal reorganization, which are hallmark features of myofibroblast differentiation. This profibrotic response was substantially attenuated by ATD treatment, as evidenced by reduced α-SMA signal intensity (Fig. 5H,I). Taken together, these findings demonstrate that ATD effectively inhibits TGF-β-induced fibrotic activation of spinal cord fibroblasts.

3.5 ATD Inhibits TGF-β/SMAD Signaling in Fibroblasts

Following SCI, TGF-β promotes the formation of fibrosis through activation of both canonical SMAD-dependent and non-canonical signaling pathways. In this study, TGF-β stimulation was found to significantly increase the phosphorylation of SMAD2/3 in fibroblasts. ATD treatment markedly suppressed TGF-β-induced SMAD2/3 phosphorylation in a concentration-dependent manner (Fig. 6A–C). Within the TGF-β/SMAD signaling cascade, SMAD4 acts as a central mediator and SMAD7 functions as an inhibitory regulator of SMAD2/3 activity. Therefore, we examined the expression levels of SMAD4 and SMAD7 following ATD treatment. ATD significantly reduced SMAD4 protein expression, while having no significant effect on SMAD7 protein (Fig. 6D–G). For all original Western blot figures of Fig. 6A,D,F, see **Supplementary Material**. These results indicate that ATD attenuates the fibrotic activation of fibroblasts primarily by suppressing the canonical TGF-β/SMAD pathway.

4. Discussion

This study employed a well-established mouse model of SCI to systematically investigate the inhibitory effect of ATD on fibrotic scar formation, as well as the underlying mechanisms. *In vivo*, intraperitoneal administration of ATD significantly reduced the fibrotic scar area at the lesion site, suppressed the expression of glial scar and fibrosis-related markers, and promoted the recovery of hindlimb motor function in mice. *In vitro*, ATD effectively inhibited TGF-β–induced activation of spinal fibroblasts, downregulated the expression of α-SMA and Col1α1, and blocked the fibrotic cascade by suppressing SMAD2/3 phosphorylation in the TGF-β/SMAD signaling pathway. To the best of our knowledge, this is the first study to demonstrate that ATD attenuates fibrotic scar formation after SCI through direct targeting of the TGF-β/SMADs pathway. Our findings suggest a potential novel therapeutic target and provide robust experimental evidence for the clinical management of SCI.

Fibrotic scar formation constitutes a dynamic and multicellular pathological process driven primarily by the aberrant activation of pro-fibrotic signaling within the injured microenvironment following SCI. The acute injury phase is characterized by widespread death of neuronal and glial cells, thereby propagating the release of damage-associated molecular patterns (DAMPs). These molecules recruit and activate microglia/macrophages, prompting them to secrete pro-inflammatory mediators such as TGF-β and PDGF, which in turn drive the activation of astrocytes and fibroblasts [31–33]. Under sustained TGF-β stimulation, fibroblasts undergo phenotypic transition characterized by α-SMA expression and robust secretion of ECM components, including type I collagen, fibronectin, and chondroitin sulfate proteoglycans (CSPGs). This ultimately leads to the formation of a dense fibro-gliotic scar complex at the pe-

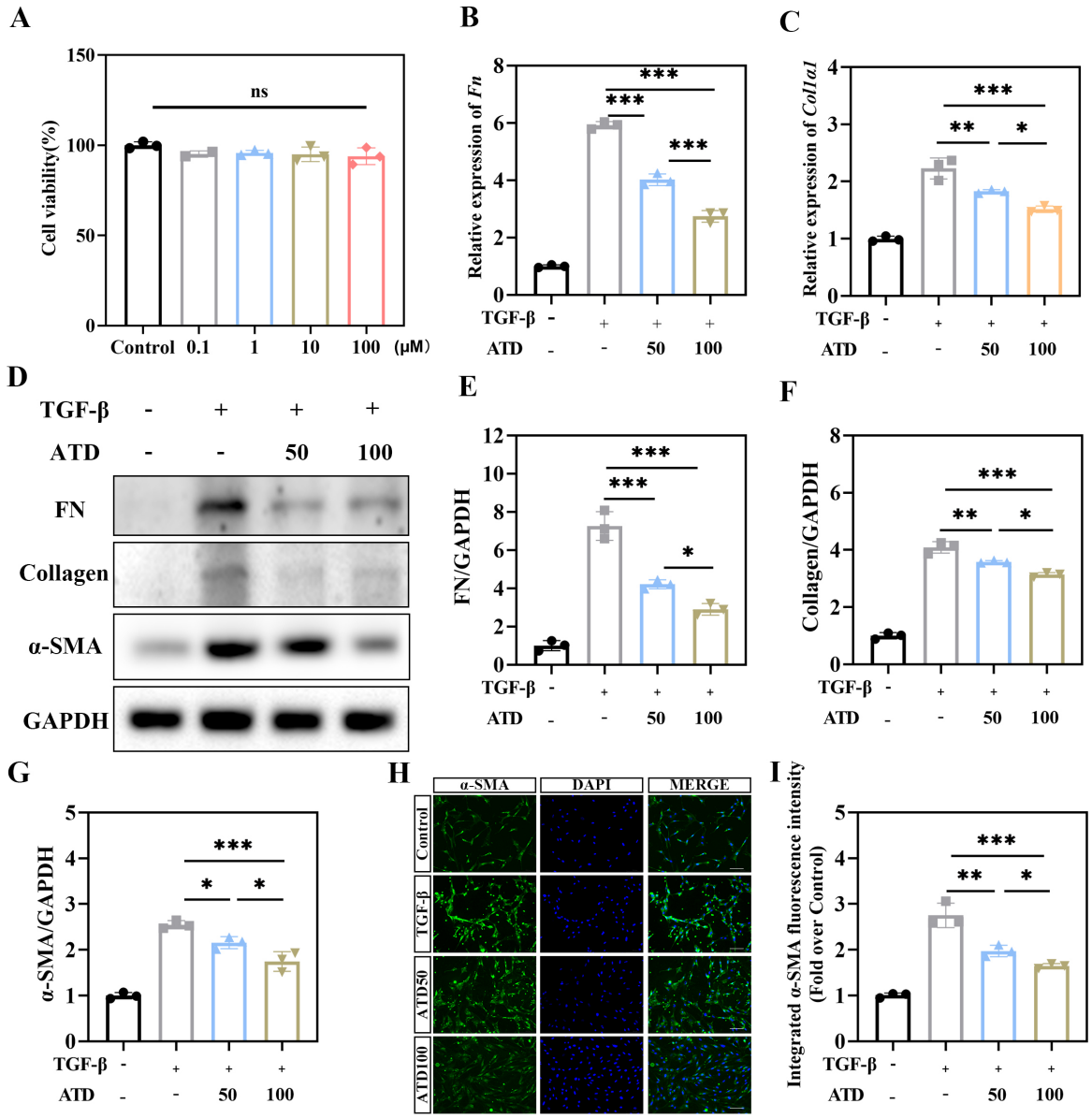

Fig. 5. ATD inhibits TGF-β-induced fibrotic activation in spinal cord fibroblasts. (A) Cytotoxicity of various concentrations of ATD was assessed using the CCK-8 assay (n = 3). (B,C) Quantitative real-time PCR (qPCR) analysis revealed that ATD treatment significantly suppressed TGF-β-induced mRNA expression of fibronectin (*Fn*) (B) and collagen type I alpha 1 (*Col1*α*1*) (C) in mouse spinal cord fibroblasts (n = 3). (D–G) Western blot analysis showed reduced protein levels of FN (E), collagen (F), and α-SMA (G) in ATD-treated cells compared to Vehicle controls, with quantification shown in panels E, F, and G respectively (n = 3). (H,I) Immunofluorescence staining confirmed downregulation of α-SMA expression in ATD-treated fibroblasts, with representative images shown in (H) and quantitative analysis in (I) (n = 3; scale bar = 50 μm). Data shown are the mean ± SEM, *$p < 0.05$, **$p < 0.01$, ***$p < 0.001$, ns $p > 0.05$.

riphery of the injury site [34,35]. The scar serves as a physical barrier that impedes axonal regeneration, while exacerbating neural repair failure by releasing inhibitory molecules and sustaining a pro-inflammatory microenvironment [36]. The present study found that ATD significantly reduces TGF-β1 expression in the lesion area and inhibits SMAD2/3 phosphorylation, indicating a central regulatory role of the TGF-β/SMAD signaling pathway in fibrotic scar formation. Interruption of this pathway effectively attenuates scar deposition, thereby providing a well-defined molecular target for therapeutic intervention in post-SCI fibrosis.

A vicious cycle of bidirectional regulation occurs between fibrous scar formation and neuronal death. On the one hand, fibroblasts and activated astrocytes in the scar continuously secrete pro-inflammatory factors and neuro-

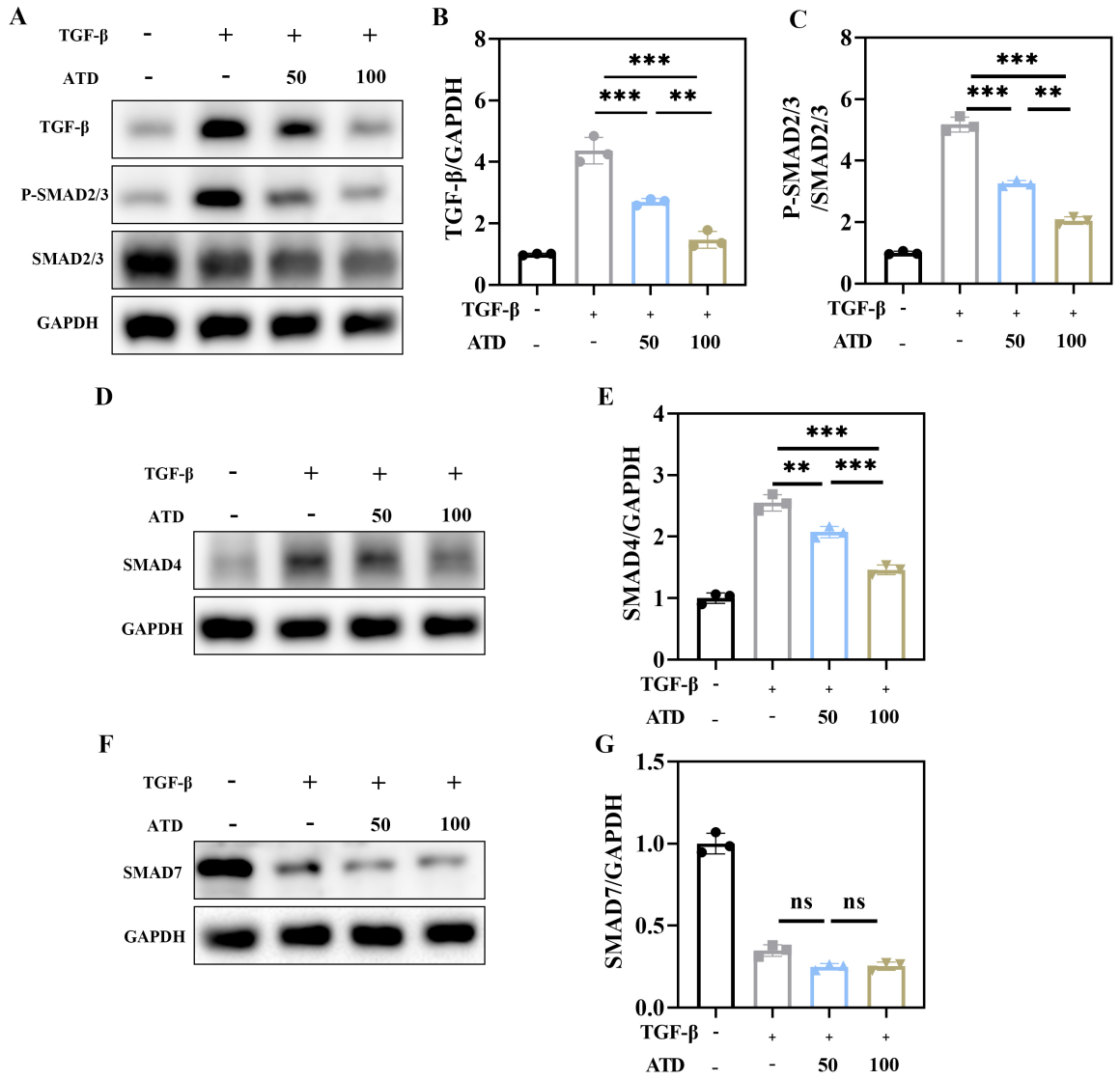

Fig. 6. ATD inhibits the TGF-β/SMAD signaling pathway in fibroblasts. (A) Representative western blot images of protein expression in TGF-β-induced mouse spinal cord fibroblasts. (B) Quantitative analysis of TGF-β expression levels. (C) Quantitative analysis of phosphorylated SMAD2/3 (P-SMAD2/3) and total SMAD2/3 levels. Data are from three independent experiments (n = 3). (D,E) The expression of SMAD4 was similarly evaluated by Western blot and quantified (n = 3). (F,G) SMAD7 protein expression was also examined by Western blot and subjected to quantitative analysis (n = 3). Data shown are the mean $\pm$ SEM, ns $p > 0.05$, $^{**}p < 0.01$, $^{***}p < 0.001$.

toxic molecules to directly induce neuronal apoptosis [37, 38]. On the other hand, excessive accumulation of ECM within the fibrotic scar disrupts the blood-spinal cord barrier in the lesion site, impedes the delivery of neurotrophic factors, and exacerbates neuronal ischemia and hypoxia via mechanical compression [39]. ATD treatment after SCI significantly reduced neuronal pyknosis and apoptosis and increased the number of Neun positive neurons, which may be due to an improved local microenvironment following inhibition of fibrous scar formation. In addition, CSPGs in fibrous scars inhibit axonal regeneration and induce growth cone collapse by binding to neuronal surface receptors, while ATD indirectly attenuates the inhibitory effects on neuronal survival and axon repair by reducing the scar area and deposition of CSPGs [40]. In the current study, the number of serotonergic axons passing through the scar area was significantly increased in the ATD treatment group, further confirming that inhibition of the fibrous scar can promote neuronal survival and reconstruction of functional connectivity by improving the neural microenvironment.

TGF-β family members, especially TGF-β1, play key regulatory roles in fibrotic diseases. They regulate the activation, proliferation, and ECM metabolism of fibroblasts by activating both classical SMAD2/3/4 and non-classical pathways, such as MAPK and PI3K/Akt [41–43]. In SCI, the abnormally high expression of TGF-β1 is positively

correlated with the degree of scar formation and the prognosis of neurological function [21,22]. The present study found that the level of TGF-β1 in the injured area was significantly increased after SCI. This promoted the phosphorylation and subsequent nuclear translocation of SMAD2/3. Consequently, the transcription of fibrosis-related genes, including *Col1*α*1* and *Fn*, was initiated in fibroblasts. ATD blocks the pro-fibrotic signal transduction of TGF-β1 by inhibiting the phosphorylation and nuclear localization of SMAD2/3, but does not affect the expression of SMAD4 and SMAD7, suggesting that its target is the receptor kinases or related co-regulators upstream of SMAD2/3. It is worth noting that the research on the TGF-β/SMADs pathway in liver, kidney and lung fibrosis is relatively mature, but its regulatory network in neural fibrosis still requires further exploration. While the present study demonstrates that ATD treatment effectively attenuates fibrotic scarring and promotes functional recovery after SCI, and our *in vitro* data align these benefits with the modulation of the TGF-β/SMAD signaling axis in fibroblasts, a key mechanistic question remains open. However, our work does not yet provide direct *in vivo* evidence that inhibiting the TGF-β/SMAD pathway within the injured spinal cord is necessary and sufficient to recapitulate ATD's therapeutic effects. Establishing such definitive causal proof, through the use of conditional genetic models or localized pharmacological inhibition of SMAD4, represents a crucial next step. This validation is technically demanding, as it requires precise spatial and temporal control within the complex injury milieu to avoid confounding systemic effects. The current findings therefore position the TGF-β/SMAD pathway as a strongly implicated, but not conclusively proven, primary mediator of ATD's action *in vivo*. Addressing this specific gap through the suggested functional rescue or mimicry experiments will be a central objective of our subsequent research, aiming to transition the observed correlation into a firmly established mechanism.

ATD, an active constituent of the traditional Chinese medicinal herb Atractylodes, has been previously reported to exert multiple pharmacological activities, including anti-inflammatory, metabolic regulatory, and anti-fibrotic effects [24–27]. The therapeutic potential of bioactive compounds derived from Atractylodes species in central nervous system disorders, including SCI, is gaining recognition. Notably, atractylenolide III, a sesquiterpene lactone from the same genus, has demonstrated efficacy in experimental SCI, primarily by modulating neuroinflammatory responses involving microglia/macrophages [44]. While this prior work provides valuable context, our study introduces atractylodin—a chemically distinct polyacetylene from Atractylodes—and defines its unique therapeutic niche. Unlike the established anti-inflammatory profile of atractylenolides, our investigation is the first to systematically establish atractylodin's potency in specifically mitigating fibrotic scar formation, a pivotal and mechanically obstructive pathology in the subacute to chronic phases of SCI. The chemical distinction between these compound classes suggests divergent molecular interactions and target profiles. Our focus on the TGF-β/Smad pathway for atractylodin is justified by its central role in fibrosis and is supported by our mechanistic data. This focus does not duplicate but rather complements the existing pharmacological understanding of Atractylodes-derived compounds. By elucidating atractylodin's anti-fibrotic action, our work expands the therapeutic scope of this medicinal genus, highlighting how different constituents may target sequential or parallel pathological events in SCI—from acute inflammation to chronic fibrosis. This positions atractylodin as a promising candidate for combination strategies or for intervention in the fibrotic phase of injury, addressing an unmet need distinct from acute neuroinflammation management.

In the current study, ATD showed a significant inhibitory effect on fibrosis after SCI. The mechanism of action was different from that of traditional anti-inflammatory drugs, and was achieved by specifically interfering with the TGF-β/SMADs pathway. *In vitro* experiments demonstrated that ATD suppresses TGF-β-induced fibroblast activation and reduces ECM production. This mechanism differs notably from the previously described effect of ATD in lung fibrosis, where it stabilizes vimentin to inhibit TGF-β1 recycling. Hence, different fibrotic contexts may have tissue-specific modes of action for ATD. Furthermore, *in vivo* administration of high-dose ATD resulted in enhanced suppression of scar formation and significant improvement in motor function. While our initial histological examination of major organs revealed no apparent morphological damage, the serum data provide a functional perspective on systemic biocompatibility. The absence of significant changes in ALT, AST, CRE, and BUN levels in ATD-treated animals offers direct evidence that the compound, at doses effective in reducing scar formation and promoting functional recovery, places no detectable functional burden on the liver and kidneys. This combined assessment establishes a foundational safety dataset supporting the further preclinical development of ATD, thus supporting its potential for safe clinical translation. This study broadens the known pharmacological spectrum of ATD and represents its first application in the field of neural trauma, while revealing its novel function as a TGF-β/SMADs pathway inhibitor.

5. Limitation

This study has several limitations that warrant careful consideration. First, although our in vitro data demonstrate that ATD suppresses SMAD2/3 phosphorylation, its direct molecular target remains unknown. It is unclear whether ATD acts directly on TGF-β receptors or modulates upstream regulatory components. These questions could be addressed through targeted approaches such as drug affinity chromatography, cellular thermal shift assays,

or structure-guided molecular docking. Second, our investigation centered predominantly on fibroblasts. However, fibrotic scar formation is a multicellular process involving dynamic crosstalk among astrocytes, pericytes, microglia and macrophages, and infiltrating immune cells. The impact of ATD on these non-fibroblast populations, and how it influences intercellular signaling networks that drive scar maturation, was not assessed. Third, although ATD significantly reduced fibrotic scar area, the functional relevance of this reduction for axonal regeneration was inferred indirectly from neurofilament and βIII-tubulin immunoreactivity. Critically, direct anatomical evidence remains absent, such as anterograde tracing showing regenerating axons traversing the lesion core or synaptic marker colocalization at distal targets. Fourth, the therapeutic window for ATD administration was not systematically evaluated. Although we initiated treatment immediately after injury, the efficacy of delayed intervention, which would be more reflective of real-world clinical scenarios, has not been tested. Finally, although ATD originates from traditional Chinese medicine, its pharmacokinetic profile, including central nervous system penetration, bioavailability following systemic administration, and long-term safety after spinal cord injury, remain uncharacterized. These knowledge gaps currently constrain its translational feasibility.

6. Conclusions

In summary, our data indicate that ATD acts as an effective inhibitor of the TGF-β/SMADs pathway in fibroblasts, thereby attenuating fibrosis and limiting fibrotic scar deposition after SCI. Together, these effects contribute to improved functional recovery, as ATD reduces the scar area, supports axon regrowth, and enhances motor performance in a mouse model of SCI.

Availability of Data and Materials

The data used to support the findings of this study are available from the corresponding author upon request.

Author Contributions

CLS supervised the research. ZWL, CF and CLS designed and performed the experiments, ZWL interpreted the data and wrote the manuscript. CCF, ZMW, and CHZ analyzed the data. All authors critically reviewed and revised the academic content of the article. All authors read and approved the final manuscript. All authors have participated sufficiently in the work and agreed to be accountable for all aspects of the work.

Ethics Approval and Consent to Participate

All animal experimental protocols were reviewed and approved by the Anhui Medical University Ethics Committee (LLSC20242471) in accordance with the ARRIVE guidelines and the National Institutes of Health Guide for the Care and Use of Laboratory Animals.

Acknowledgment

We would like to thank the Center for Scientific Research of Anhui Medical University for valuable help in our experiment.

Funding

This research received no external funding.

Conflict of Interest

The authors declare no conflict of interest.

Supplementary Material

Supplementary material associated with this article can be found, in the online version, at https://doi.org/10.31083/JIN47565.

References

[1] Li D, Lu X, Xu G, Liu S, Gong Z, Lu F, *et al*. Dihydroorotate dehydrogenase regulates ferroptosis in neurons after spinal cord injury via the P53-ALOX15 signaling pathway. CNS Neuroscience & Therapeutics. 2023; 29: 1923–1939. https://doi.org/10.1111/cns.14150.

[2] Shao A, Tu S, Lu J, Zhang J. Crosstalk between stem cell and spinal cord injury: pathophysiology and treatment strategies. Stem Cell Research & Therapy. 2019; 10: 238. https://doi.org/10.1186/s13287-019-1357-z.

[3] Hellenbrand DJ, Quinn CM, Piper ZJ, Morehouse CN, Fixel JA, Hanna AS. Inflammation after spinal cord injury: a review of the critical timeline of signaling cues and cellular infiltration. Journal of Neuroinflammation. 2021; 18: 284. https://doi.org/10.1186/s12974-021-02337-2.

[4] Fan H, Tang HB, Chen Z, Wang HQ, Zhang L, Jiang Y, *et al*. Inhibiting HMGB1-RAGE axis prevents pro-inflammatory macrophages/microglia polarization and affords neuroprotection after spinal cord injury. Journal of Neuroinflammation. 2020; 17: 295. https://doi.org/10.1186/s12974-020-01973-4.

[5] Chang J, Qian Z, Wang B, Cao J, Zhang S, Jiang F, *et al*. Transplantation of A2 type astrocytes promotes neural repair and remyelination after spinal cord injury. Cell Communication and Signaling: CCS. 2023; 21: 37. https://doi.org/10.1186/s12964-022-01036-6.

[6] Clifford T, Finkel Z, Rodriguez B, Joseph A, Cai L. Current Advancements in Spinal Cord Injury Research-Glial Scar Formation and Neural Regeneration. Cells. 2023; 12: 853. https://doi.org/10.3390/cells12060853.

[7] Xue X, Wu X, Fan Y, Han S, Zhang H, Sun Y, *et al*. Heterogeneous fibroblasts contribute to fibrotic scar formation after spinal cord injury in mice and monkeys. Nature Communications. 2024; 15: 6321. https://doi.org/10.1038/s41467-024-50564-x.

[8] Tran AP, Warren PM, Silver J. Regulation of autophagy by inhibitory CSPG interactions with receptor PTPσ and its impact on plasticity and regeneration after spinal cord injury. Experimental Neurology. 2020; 328: 113276. https://doi.org/10.1016/j.expneurol.2020.113276.

[9] Francos-Quijorna I, Sánchez-Petidier M, Burnside ER, Badea SR, Torres-Espin A, Marshall L, *et al*. Chondroitin sulfate proteoglycans prevent immune cell phenotypic conversion and in-

flammation resolution via TLR4 in rodent models of spinal cord injury. Nature Communications. 2022; 13: 2933. https://doi.org/10.1038/s41467-022-30467-5.

[10] Chen X, Zhang L, Hua F, Zhuang Y, Liu H, Wang S. EphA4 Obstructs Spinal Cord Neuron Regeneration by Promoting Excessive Activation of Astrocytes. Cellular and Molecular Neurobiology. 2022; 42: 1557–1568. https://doi.org/10.1007/s10571-021-01046-x.

[11] Nogueira-Rodrigues J, Leite SC, Pinto-Costa R, Sousa SC, Luz LL, Sintra MA, *et al*. Rewired glycosylation activity promotes scarless regeneration and functional recovery in spiny mice after complete spinal cord transection. Developmental Cell. 2022; 57: 440–450.e7. https://doi.org/10.1016/j.devcel.2021.12.008.

[12] Shan F, Ye J, Xu X, Liang C, Zhao Y, Wang J, *et al*. Galectin-3 inhibition reduces fibrotic scarring and promotes functional recovery after spinal cord injury in mice. Cell & Bioscience. 2024; 14: 128. https://doi.org/10.1186/s13578-024-01310-9.

[13] Fan W, Qu Y, Yuan X, Shi H, Liu G. Loureirin B Accelerates Diabetic Wound Healing by Promoting TGFβ/Smad-Dependent Macrophage M2 Polarization: A Concerted Analytical Approach Through Single-Cell RNA Sequencing and Experimental Verification. Phytotherapy Research. 2025; 39: 5450–5463. https://doi.org/10.1002/ptr.8373.

[14] Li Y, Guo F, Huang R, Ma L, Fu P. Natural flavonoid pectolinarigenin alleviated kidney fibrosis via inhibiting the activation of TGFβ/SMAD3 and JAK2/STAT3 signaling. International Immunopharmacology. 2021; 91: 107279. https://doi.org/10.1016/j.intimp.2020.107279.

[15] Cui J, Zhang S, Acharya K, Xu Y, Guo H, Li T, *et al*. Decorin attenuates hypertrophic scar fibrosis via TGFβ/Smad signalling. Experimental Dermatology. 2024; 33: e15133. https://doi.org/10.1111/exd.15133.

[16] Khongpiroon C, Buakaew W, Brindley PJ, Potikanond S, Daowtak K, Thongsri Y, *et al*. Anti-Fibrotic Effect of Oleamide Identified from the *Moringa oleifera* Lam. Leaves via Inhibition of TGF-β1-Induced SMAD2/3 Signaling Pathway. International Journal of Molecular Sciences. 2025; 26: 3388. https://doi.org/10.3390/ijms26073388.

[17] Liu YY, Shi Y, Liu Y, Pan XH, Zhang KX. Telomere shortening activates TGF-β/Smads signaling in lungs and enhances both lipopolysaccharide and bleomycin-induced pulmonary fibrosis. Acta Pharmacologica Sinica. 2018; 39: 1735–1745. https://doi.org/10.1038/s41401-018-0007-9.

[18] Zhang G, Jiang Y, Liu X, Deng Y, Wei B, Shi L. Lingonberry Anthocyanins Inhibit Hepatic Stellate Cell Activation and Liver Fibrosis via TGFβ/Smad/ERK Signaling Pathway. Journal of Agricultural and Food Chemistry. 2021; 69: 13546–13556. https://doi.org/10.1021/acs.jafc.1c05384.

[19] Wan R, Wang L, Duan Y, Zhu M, Li W, Zhao M, *et al*. ADRB2 inhibition combined with antioxidant treatment alleviates lung fibrosis by attenuating TGFβ/SMAD signaling in lung fibroblasts. Cell Death Discovery. 2023; 9: 407. https://doi.org/10.1038/s41420-023-01702-9.

[20] Liu Y, Wei J, Li Z, Huang S, Chen M, Yu C, *et al*. Shenqi Wan inhibits cellular senescence to alleviate renal fibrosis by modulating the AQP1/TGF-β1/ITPR1 axis. Phytomedicine: International Journal of Phytotherapy and Phytopharmacology. 2025; 147: 157201. https://doi.org/10.1016/j.phymed.2025.157201.

[21] Jin Z, Tian L, Zhang Y, Zhang X, Kang J, Dong H, *et al*. Apigenin inhibits fibrous scar formation after acute spinal cord injury through TGFβ/SMADs signaling pathway. CNS Neuroscience & Therapeutics. 2022; 28: 1883–1894. https://doi.org/10.1111/cns.13929.

[22] Xu Y, He X, Wang Y, Jian J, Peng X, Zhou L, *et al*. 5-Fluorouracil reduces the fibrotic scar via inhibiting matrix metalloproteinase 9 and stabilizing microtubules after spinal cord injury. CNS Neuroscience & Therapeutics. 2022; 28: 2011–2023. https://doi.org/10.1111/cns.13930.

[23] Chen L, Zhang S, Wang Y, Sun H, Wang S, Wang D, *et al*. Integrative analysis of transcriptome and metabolome reveals the sesquiterpenoids and polyacetylenes biosynthesis regulation in Atractylodes lancea (Thunb.) DC. International Journal of Biological Macromolecules. 2023; 253: 127044. https://doi.org/10.1016/j.ijbiomac.2023.127044.

[24] Yu C, Xiong Y, Chen D, Li Y, Xu B, Lin Y, *et al*. Ameliorative effects of atractylodin on intestinal inflammation and co-occurring dysmotility in both constipation and diarrhea prominent rats. The Korean Journal of Physiology & Pharmacology. 2017; 21: 1–9. https://doi.org/10.4196/kjpp.2017.21.1.1.

[25] Qu L, Lin X, Liu C, Ke C, Zhou Z, Xu K, *et al*. Atractylodin Attenuates Dextran Sulfate Sodium-Induced Colitis by Alleviating Gut Microbiota Dysbiosis and Inhibiting Inflammatory Response Through the MAPK Pathway. Frontiers in Pharmacology. 2021; 12: 665376. https://doi.org/10.3389/fphar.2021.665376.

[26] Chuang CH, Cheng YC, Lin SC, Lehman CW, Wang SP, Chen DY, *et al*. Atractylodin Suppresses Dendritic Cell Maturation and Ameliorates Collagen-Induced Arthritis in a Mouse Model. Journal of Agricultural and Food Chemistry. 2019; 67: 6773–6784. https://doi.org/10.1021/acs.jafc.9b01163.

[27] Lyu Z, Ji X, Chen G, An B. Atractylodin ameliorates lipopolysaccharide and d-galactosamine-induced acute liver failure via the suppression of inflammation and oxidative stress. International Immunopharmacology. 2019; 72: 348–357. https://doi.org/10.1016/j.intimp.2019.04.005.

[28] Song GY, Kim SM, Back S, Yang SB, Yang YM. *Atractylodes Lancea* and Its Constituent, Atractylodin, Ameliorates Metabolic Dysfunction-Associated Steatotic Liver Disease via AMPK Activation. Biomolecules & Therapeutics. 2024; 32: 778–792. https://doi.org/10.4062/biomolther.2024.083.

[29] Song MY, Lim SK, Wang JH, Kim H. The Root of Atractylodes macrocephala Koidzumi Prevents Obesity and Glucose Intolerance and Increases Energy Metabolism in Mice. International Journal of Molecular Sciences. 2018; 19: 278. https://doi.org/10.3390/ijms19010278.

[30] Hao M, Guan Z, Zhang Z, Ai H, Peng X, Zhou H, *et al*. Atractylodinol prevents pulmonary fibrosis through inhibiting TGF-β receptor 1 recycling by stabilizing vimentin. Molecular Therapy: the Journal of the American Society of Gene Therapy. 2023; 31: 3015–3033. https://doi.org/10.1016/j.ymthe.2023.08.017.

[31] Al Mamun A, Wu Y, Monalisa I, Jia C, Zhou K, Munir F, *et al*. Role of pyroptosis in spinal cord injury and its therapeutic implications. Journal of Advanced Research. 2020; 28: 97–109. https://doi.org/10.1016/j.jare.2020.08.004.

[32] Yao F, Luo Y, Liu YC, Chen YH, Li YT, Hu XY, *et al*. Imatinib inhibits pericyte-fibroblast transition and inflammation and promotes axon regeneration by blocking the PDGF-BB/PDGFRβ pathway in spinal cord injury. Inflammation and Regeneration. 2022; 42: 44. https://doi.org/10.1186/s41232-022-00223-9.

[33] Ma CW, Wang ZQ, Ran R, Liao HY, Lyu JY, Ren Y, *et al*. TGF-β signaling pathway in spinal cord injury: Mechanisms and therapeutic potential. Journal of Neuroscience Research. 2024; 102: e25255. https://doi.org/10.1002/jnr.25255.

[34] Milich LM, Choi JS, Ryan C, Cerqueira SR, Benavides S, Yahn SL, *et al*. Single-cell analysis of the cellular heterogeneity and interactions in the injured mouse spinal cord. The Journal of Experimental Medicine. 2021; 218: e20210040. https://doi.org/10.1084/jem.20210040.

[35] Gong L, Gu Y, Han X, Luan C, Liu C, Wang X, *et al*. Spatiotemporal Dynamics of the Molecular Expression Pattern and Intercellular Interactions in the Glial Scar Response to Spinal Cord Injury. Neuroscience Bulletin. 2023; 39: 213–244. https:

//doi.org/10.1007/s12264-022-00897-8.

[36] Tamaru T, Kobayakawa K, Saiwai H, Konno D, Kijima K, Yoshizaki S, *et al*. Glial scar survives until the chronic phase by recruiting scar-forming astrocytes after spinal cord injury. Experimental Neurology. 2023; 359: 114264. https://doi.org/10.1016/j.expneurol.2022.114264.

[37] Riew TR, Kim S, Jin X, Kim HL, Yoo K, Seo SB, *et al*. Induction of BIS Protein During Astroglial and Fibrotic Scar Formation After Mitochondrial Toxin-Mediated Neuronal Injury in Rats. Molecular Neurobiology. 2020; 57: 3846–3859. https://doi.org/10.1007/s12035-020-02000-6.

[38] Rong Y, Ji C, Wang Z, Ge X, Wang J, Ye W, *et al*. Small extracellular vesicles encapsulating CCL2 from activated astrocytes induce microglial activation and neuronal apoptosis after traumatic spinal cord injury. Journal of Neuroinflammation. 2021; 18: 196. https://doi.org/10.1186/s12974-021-02268-y.

[39] Qian D, Xu J, Zhang X, Hu F, Cao S, Dong Y, *et al*. Microenvironment Self-Adaptive Nanomedicine Promotes Spinal Cord Repair by Suppressing Inflammation Cascade and Neural Apoptosis. Advanced Materials (Deerfield Beach, Fla.). 2024; 36: e2307624. https://doi.org/10.1002/adma.202307624.

[40] Ahmed MC, Kakunuri T, Peris L, Meffre D, Yilmaz EN, Grewing L, *et al*. The inflammatory APRIL (a proliferation-inducing ligand) antagonizes chondroitin sulphate proteoglycans to promote axonal growth and myelination. Brain Communications. 2025; 7: fcae473. https://doi.org/10.1093/braincomms/fcae473.

[41] Li N, Wang Z, Sun T, Lei Y, Liu X, Li Z. Apigenin Alleviates Renal Fibroblast Activation through AMPK and ERK Signaling Pathways *In Vitro*. Current Pharmaceutical Biotechnology. 2020; 21: 1107–1118. https://doi.org/10.2174/1389201021666200320140908.

[42] Cai Z, Guo H, Qian J, Liu W, Li Y, Yuan L, *et al*. Effects of bone morphogenetic protein 4 on TGF-β1-induced cell proliferation, apoptosis, activation and differentiation in mouse lung fibroblasts *via* ERK/p38 MAPK signaling pathway. PeerJ. 2022; 10: e13775. https://doi.org/10.7717/peerj.13775.

[43] Tang Q, Markby GR, MacNair AJ, Tang K, Tkacz M, Parys M, *et al*. TGF-β-induced PI3K/AKT/mTOR pathway controls myofibroblast differentiation and secretory phenotype of valvular interstitial cells through the modulation of cellular senescence in a naturally occurring in vitro canine model of myxomatous mitral valve disease. Cell Proliferation. 2023; 56: e13435. https://doi.org/10.1111/cpr.13435.

[44] Xue MT, Sheng WJ, Song X, Shi YJ, Geng ZJ, Shen L, *et al*. Atractylenolide III ameliorates spinal cord injury in rats by modulating microglial/macrophage polarization. CNS Neuroscience & Therapeutics. 2022; 28: 1059–1071. https://doi.org/10.1111/cns.13839.